

Large Point-to-Gaussian Model for Image-to-3D Generation

Longfei Lu*
Tsinghua Shenzhen International
Graduate School, Tsinghua University
Shenzhen, China
loneffy.lu@gmail.com

Huachen Gao*
Tencent, Hunyuan
Shenzhen, China
gaohuachen712@gmail.com

Tao Dai†
College of Computer Science and
Software Engineering, Shenzhen
University
Shenzhen, China
daitao.edu@gmail.com

Yaohua Zha
Tsinghua Shenzhen International
Graduate School, Tsinghua University
Shenzhen, China
zyh1614399882@gmail.com

Zhi Hou
Junta Wu
Tencent, Hunyuan
Shenzhen, China
{houzhi91,juntawu41}@gmail.com

Shu-Tao Xia
Tsinghua Shenzhen International
Graduate School, Tsinghua University
Peng Cheng Laboratory
Shenzhen, China
xiast@sz.tsinghua.edu.cn

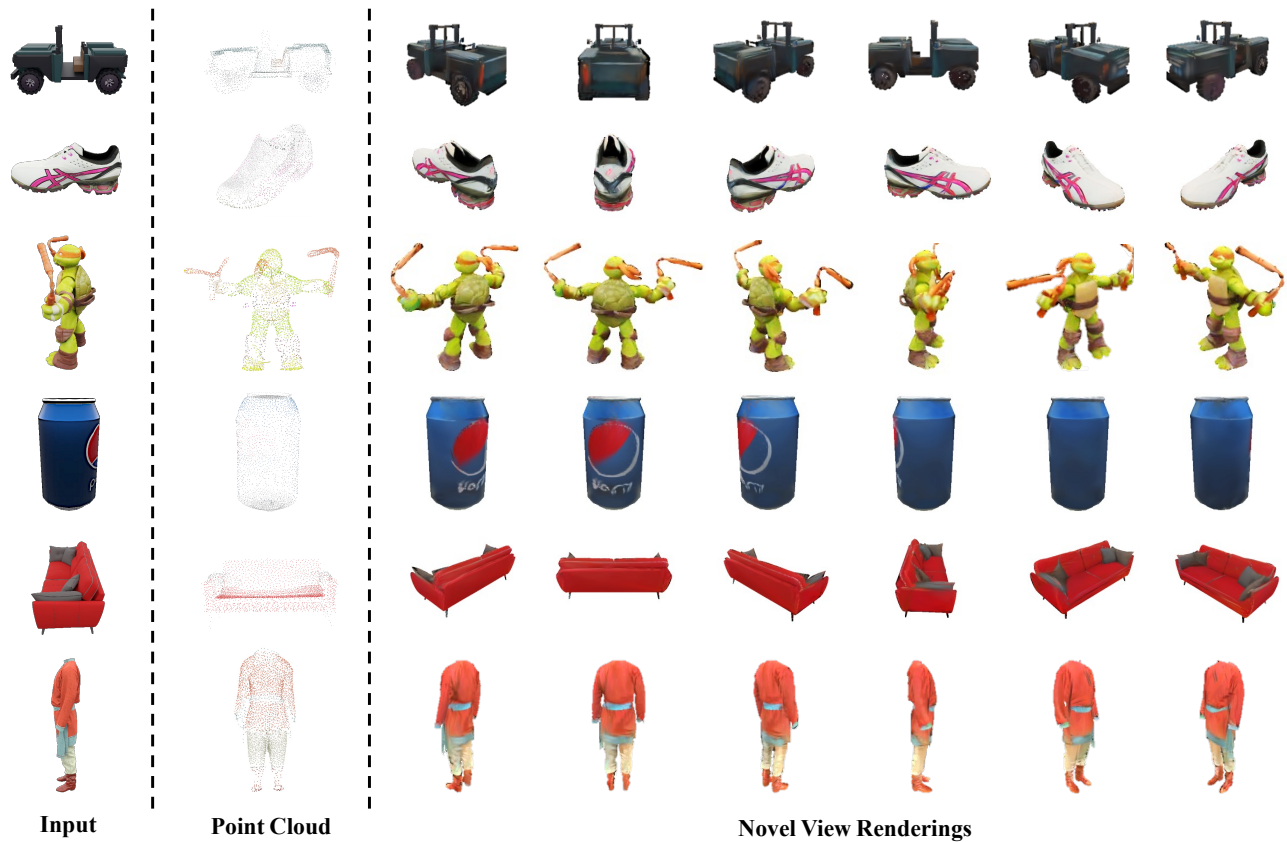


Figure 1: Our method produces high-fidelity generation results from a single-view image.

*These authors contributed equally to this work.

†Corresponding author: Tao Dai (daitao.edu@gmail.com)

Permission to make digital or hard copies of all or part of this work for personal or classroom use is granted without fee provided that copies are not made or distributed for profit or commercial advantage and that copies bear this notice and the full citation on the first page. Copyrights for components of this work owned by others than the author(s) must be honored. Abstracting with credit is permitted. To copy otherwise, or

republish, to post on servers or to redistribute to lists, requires prior specific permission and/or a fee. Request permissions from permissions@acm.org.

MM '24, October 28–November 1, 2024, Melbourne, VIC, Australia

© 2024 Copyright held by the owner/author(s). Publication rights licensed to ACM.

ACM ISBN 979-8-4007-0686-8/24/10

<https://doi.org/10.1145/3664647.3680920>

Abstract

Recently, image-to-3D approaches have significantly advanced the generation quality and speed of 3D assets based on large reconstruction models, particularly 3D Gaussian reconstruction models. Existing large 3D Gaussian models directly map 2D image to 3D Gaussian parameters, while regressing 2D image to 3D Gaussian representations is challenging without 3D priors. In this paper, we propose a large Point-to-Gaussian model, that inputs the initial point cloud produced from large 3D diffusion model conditional on 2D image to generate the Gaussian parameters, for image-to-3D generation. The point cloud provides initial 3D geometry prior for Gaussian generation, thus significantly facilitating image-to-3D Generation. Moreover, we present the Attention mechanism, Projection mechanism, and Point feature extractor, dubbed as **APP** block, for fusing the image features with point cloud features. The qualitative and quantitative experiments extensively demonstrate the effectiveness of the proposed approach on GSO and Objaverse datasets, and show the proposed method achieves state-of-the-art performance.

CCS Concepts

• **Information systems** → **Multimedia content creation**; • **Computing methodologies** → **Appearance and texture representations**; **Virtual reality**.

Keywords

3D Generation, 3D Gaussian Splatting, Single-View Reconstruction, Point Cloud

ACM Reference Format:

Longfei Lu, Huachen Gao, Tao Dai, Yaohua Zha, Zhi Hou, Junta Wu, and Shu-Tao Xia. 2024. Large Point-to-Gaussian Model for Image-to-3D Generation. In *Proceedings of the 32nd ACM International Conference on Multimedia (MM '24)*, October 28–November 1, 2024, Melbourne, VIC, Australia. ACM, New York, NY, USA, 10 pages. <https://doi.org/10.1145/3664647.3680920>

1 Introduction

Generating high-quality 3D assets from images is a pivotal task in numerous fields, notably in gaming, film production, and VR/AR, etc. The learning-based 3D generation algorithms [12, 38] allow rapid generation of high-quality 3D assets free of tedious manual processes and complex computer graphics tools.

Recently, the realm of 3D generation has witnessed a surge of innovative techniques, with particular prominence given to two main approaches: 2D-lifting-based generation and feed-forward generation, driving the field's progress. Following the pioneering work [38], the 2D-lifting approaches [17, 38, 54] leverages Score Distillation Sampling (SDS) [38] to distill 3D implicit representations (e.g., NeRF [33]) from large diffusion models [20, 21], while feed-forward generation approaches [12, 15, 49, 55] straightforwardly reconstruct 3D implicit representations from 2D image without iterative optimization. Compared to 2D-lifting approaches that require extensive optimization time, the feed-forward generation techniques can generate 3D assets within a few seconds. Besides, inspired by recent 3D Gaussian Splatting (3D-GS) [14] with promising rendering quality in the novel view synthesis (NVS) and fast rendering speed, the latest approaches improve the speed and quality of

3D generation by integrating the 3D-GS into 2D-lifting generation [5, 45, 56] or feed-forward generation [44, 53, 63].

The previous feed-forward approaches with 3D-GS [44, 53, 63] build mappings directly from implicit image features to Gaussian parameters. However, this regression based method is non-trivial for 3D-GS learning, given that the input 2D image does not always contain efficient 3D information for the corresponding object. By contrast, Point Cloud [57, 59, 62] is an effective 3D representation and capable of providing informative geometry priors for the generation of explicit 3D Gaussians, whilst the current large 3D diffusion model (e.g. Point-E [34]) can generate diverse and satisfying initial point cloud for the input image. Therefore, we present to generate Gaussian parameters from point cloud, dubbed as Point-to-Gaussian, to advance the 3D-GS learning for image-to-3D generation as shown in Fig. 2.

Nevertheless, it is still non-trivial to convert the coarse point cloud from 3D large models to Gaussian representations given that the generated point cloud might be sparse and noisy, which carries insufficient appearance features and inaccurate geometric structural information to provide an informative prior for precise Gaussian generation. We thus first utilize a point cloud upsampler to densify it and thus enhance the features, and then utilize a point feature extractor to extract the features from the point cloud. Besides, considering that the input image contains rich appearance information, we present to enhance the cross-modality features to fuse the 2D image representations to the 3D point cloud for facilitating the 3D representations. Specifically, we project the 3D point to 2D image according to camera pose to obtain the features. However, there are occlusions in the point cloud during the projection. We introduce an attention mechanism to selectively query features for 3D points, enhancing their representations, particularly under occlusion. Subsequently, we integrate the 3D representations obtained from the Attention mechanism, pose-aware Projection mechanism, and Point cloud feature extractor, termed APP Block, to conduct cross-modality enhancement for more effective Gaussian learning. The Gaussian parameters are finally generated using a multi-head Gaussian decoder, and the novel view images are rendered by conventional Gaussian splatting.

Our method converges quickly, which is trained only on the Objaverse-LVIS [9] subset and achieves comparable results of previous state-of-the-art methods trained with much more data, which indicates the effectiveness of the proposed method.

In summary, our main contributions are as follows:

- We propose a novel framework to generate high-quality 3D Gaussians with point cloud input. To our knowledge, our method is the first attempt to utilize the generalizable Point-to-Gaussian Generator for feed-forward image-to-3D generation.
- We introduce the Attention mechanism, Projection mechanism, and Point feature extractor as APP block into Point-to-Gaussian generator for Cross Modality Enhancement, which further integrates the geometric structural features with the 2D texture features for more effective learning.
- Qualitative and quantitative results demonstrate that our method achieves comparable performance with the previous state-of-the-art, even trained with much smaller datasets.

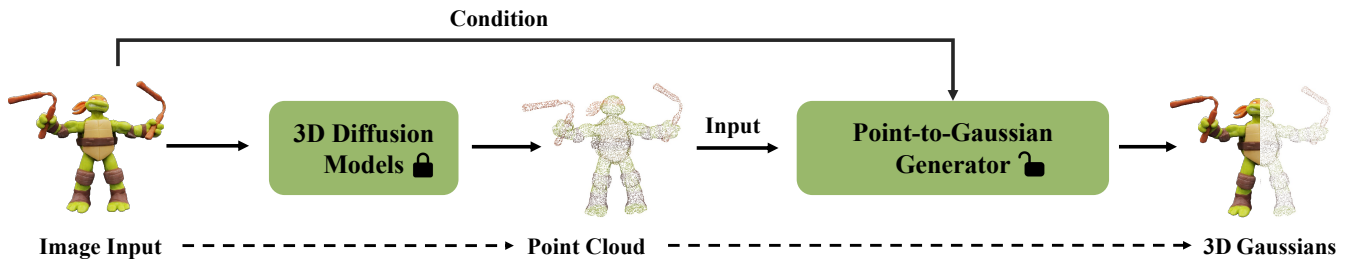


Figure 2: Illustration of our full pipeline. Given a single-view image as input, the corresponding point cloud is first generated via pre-trained 3D diffusion model [13]. Then the point cloud is sent as the input of our proposed Point-to-Gaussian Generator. The input image is introduced as complementary condition to our Gaussian generator.

2 Related Work

2.1 Diffusion Priors for 3D Generation

Recent efforts for generating 3D contents are mostly inspired from the success of 2D generative models [39]. They usually rely on Score Distillation Sampling (SDS) proposed in DreamFusion [38]. [47] interprets predictions from pretrained diffusion models as a score function of the data log-likelihood to optimize 3D representations via score matching. Subsequent work has made further enhancements based on SDS-based optimization. [17] increased the resolution of the generation, and introduced direct mesh optimizations. [51] proposed Variational Score Distillation (VSD) to enhance the quality and diversity of the generations. [54] introduced 3D shape prior from text-to-shape for better alignment between text and 3D shape. [3, 16, 40, 42] are proposed to achieve substantial improvement in quality, and further alleviate the Janus problem. [32, 45] aim to improve the optimization speed of 3D generation. Besides, many efforts [19–22, 24, 27, 41, 48] extend text-to-3D to single-view 3D generation. These methods focus on exploring non-optimization paradigms, and propose multi-view diffusion models which incorporates the information between different views for more consistent multi-view generation. Then the 3D reconstruction approaches are applied to obtain the 3D representations. [7, 46] propose to leverage video diffusion models for more consistent multi-view images.

2.2 Single-Stage 3D Generation

Unlike the SDS-based approach, the single-stage 3D generation method obtains 3D representation directly from image or text by a single feed-forward. Previous works train 3D diffusion models directly on point clouds [58] or volumes [2, 13, 34]. However, they do not generalize well to other scenes and cannot provide satisfactory textures. Recently, LRM [12] first utilizes large transformers trained on large-scale 3D datasets [8, 9] to directly predict triplane NeRF from single view in a few seconds. [49] and [15] extend the input from single-view to sparse views. [15, 55] combine the large reconstruction model with diffusion priors to achieve text-to-3D and image-to-3D generation. However, these methods utilize volume rendering based triplane NeRF as the 3D representation, which still require massive forward inferences and computation.

2.3 Gaussian Splatting in 3D Generation

3D Gaussian Splatting (3D-GS) [14] showed marvelous performance in novel view synthesis for single scene optimization [11, 33]. This representation has been applied in many downstream tasks, such as generalizable neural rendering [1, 4, 43], human reconstruction [61], and 4D generation [18], etc. Some recent works also show that 3D-GS has great potential in surface reconstructions [28–30, 36, 37]. Some concurrent works [6, 45, 56] adopt 3D-GS for SDS-based optimization to decrease generation time. In the field of single-stage 3D generation, Triplane Gaussian [63] combines LRM with 3D-GS for faster rendering speed and superior rendering quality, [53] proposes two-stage optimization with 3D-GS for high-quality generation, LGM [44] extends the single view Gaussian generation to sparse views for higher resolution. In this paper, we follow the feed-forward based image-to-3D generation scheme and propose a generalizable point-to-Gaussian model to advance the 3D-GS learning for image-to-3D generation.

3 Method

In this section, we first present the fundamental background of 3D Gaussian splatting (Section 3.1). Then, the Point to Gaussian generator, which takes the sparse point cloud generated from the pretrained 3d diffusion model and the paired images condition as inputs and outputs the 3D Gaussian representations, is introduced in (Section 3.2). To employ image conditions for further enhancing the geometric and texture features of 3D Gaussians, we present to integrate the 3D representations obtained from the Attention, Projection, and Point feature extractor, termed APP Block in (Section 3.3) to enhance the cross modality features. Lastly, the loss function and data augmentation are introduced in (Section 3.4) for optimization.

3.1 Preliminary: 3D Gaussian Splatting

3D Gaussian Splatting (3D-GS) [14] shows high-fidelity rendering quality and real-time speed in novel view synthesis (NVS), which has gained a lot of popularity. 3D-GS renders images via splatting instead of volume rendering that is commonly used in implicit representation like NeRF [33]. Specifically, 3D-GS represents scenes with a set of explicit anisotropic 3D Gaussians. Each Gaussian distribution is defined by a 3D covariance matrix Σ and a center position at point (mean) \mathcal{X} . A 3D Gaussian distribution $G(\mathcal{X})$ is

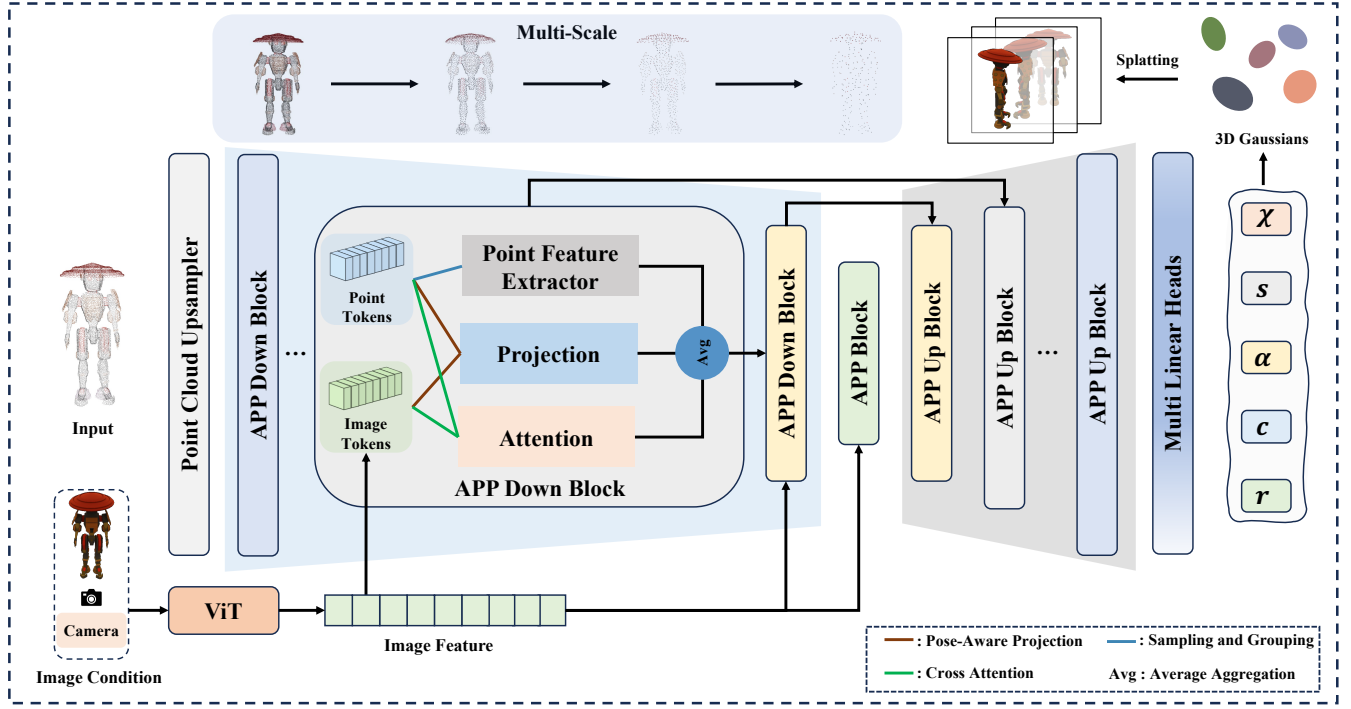


Figure 3: Detailed architecture of Point-to-Gaussian Generator. Given the input point cloud and the corresponding image, a point cloud upsampler is first applied to increase the number of 3D points, followed by an encoder consisting of several APP Down Blocks to extract the multi-scale point cloud features. Each block contains point feature extractor, projection and attention for cross modality feature enhancement. The point cloud features are decoded by a series of APP Up Blocks and Multi Linear Heads to obtain the final 3D Gaussians, and then the novel view images are obtained by conventional Gaussian splatting.

formulated as follows:

$$G(\mathcal{X}) = e^{-\frac{1}{2}\mathcal{X}^T\Sigma^{-1}\mathcal{X}}. \quad (1)$$

For more effectively optimized by gradient decent, the 3D covariance matrix Σ can be decomposed into a rotation matrix \mathbf{R} and a scaling matrix \mathbf{S} :

$$\Sigma = \mathbf{R}\mathbf{S}\mathbf{S}^T\mathbf{R}^T, \quad (2)$$

where \mathbf{R} and \mathbf{S} are two learnable parameters. During optimization, the rotation matrix R is transformed to quaternion r . Each Gaussian consists of an opacity σ and spherical harmonics (SH) coefficients c for rendering. Therefore, the complete Gaussian parameters are defined by $\mathcal{G} = \{(\mathcal{X}_i, \mathbf{S}_i, \mathbf{R}_i, \sigma_i, c_i)\}_{i=0}^n$. The Gaussians are projected from 3D space to 2D image plane for rasterization with viewing transform \mathbf{W} , the 2D covariance matrix Σ' can be computed as

$$\Sigma' = \mathbf{J}\mathbf{W}\Sigma\mathbf{W}^T\mathbf{J}^T, \quad (3)$$

where \mathbf{J} is the Jacobian of the affine approximation of the projection transformation. Finally, the color C of each pixel is accumulated by blending the overlapping Gaussians:

$$C = \sum_{i \in N} \alpha_i c_i \prod_{j=1}^{i-1} (1 - \alpha_j), \quad (4)$$

where α_j is σ_j multiplied by Σ' . The tile-based rasterizer is utilized for efficient forward and backward pass. In this paper, we reduce the degree of the SH coefficients in Gaussians to zero which represents only the diffuse color. We also remove the densification and pruning

proposed in conventional per-scene 3D-GS optimization to adapt amortized optimization.

3.2 Point to Gaussian Generator

In this section, we introduce the architecture of our Point to Gaussian Generator. As shown in Fig. 3, the Point to Gaussian Generator shares the encoder-decoder structure, which converts the point cloud to 3D Gaussians. Specifically, we leverage the point cloud generated by a pretrained diffusion model [34] for initialization, and then upsample the points with densification operation. Meanwhile, the conditional images (could be single or multi) are also incorporated to enrich the Gaussian features. Finally, a multi-head gaussian decoder is incorporated to decode the features into Gaussian parameters for splatting. Denote that the point cloud with color is of P_{N*6} , conditioning images $\{I_v\}_{v=1}^V$ and camera parameters $\{C_v\}_{v=1}^V$, the output can be formulated as

$$\mathcal{G} = \Phi(P, \{I_v\}_{v=1}^V, \{C_v\}_{v=1}^V). \quad (5)$$

Here, the $\mathcal{G} = \{(\mathcal{X}_i, \mathbf{S}_i, \mathbf{R}_i, \sigma_i, c_i)\}_{i=0}^N$ represents the N Gaussians.

3.2.1 Point Cloud Upsampler. To simplify the learning of 3D Gaussians, we utilize the point cloud as input. In single-scene optimization, as reported in the primitive 3D-GS [14], pruning and densification techniques are employed to adjust the Gaussian numbers.

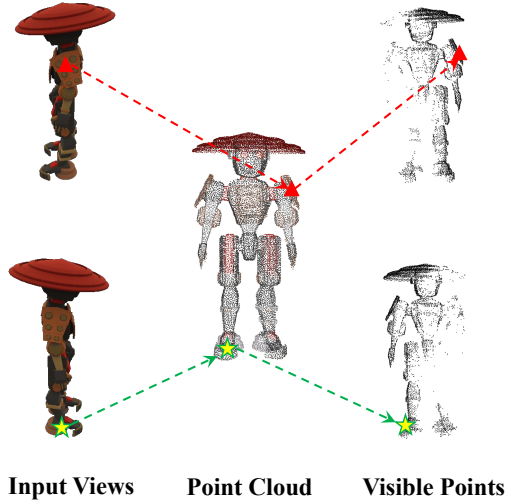


Figure 4: Visualization of pose-aware projection. The red triangle and yellow star represents the corresponding position during projection. The self-occluded view only projects to the corresponding part of the point cloud during projection.

Generally, sufficient number of 3D Gaussians can fairly represent the corresponding 3D objects, but an excess of Gaussians can also introduce computational and storage overheads. However, in the generalized 3D Gaussian framework, the gradient operates on the network, instead of the Gaussian itself, making it challenging to control and adjust the number of Gaussians dynamically. To strike a balance between performance and overhead, we initially perform a densification operation by upsampling the point cloud generated from the pretrained 3D diffusion model, thereby augmenting the number of Gaussians in the network’s final output. Specifically, we rely on the upsampling module outlined in [52] to implement a dense sampling operation on the point cloud.

3.2.2 Multi-Scale Gaussian Decoder. The Gaussian decoder’s architecture adopts a U-Net structure, akin to that described in [23]. Following densification, as detailed in Section 3.2.1, the point cloud is inputted into the network. During downsampling, the number of point clouds progressively decreases, and the current layer’s point cloud is derived via farthest point sampling (FPS) from the preceding shallower layer, thereby generating multi-scale point cloud features and expanding the receptive field. To further enrich the point cloud features and Gaussian attributes, we introduce projection and attention mechanisms for cross modality enhancement. For further elaboration, please refer to Section 3.3.

After obtaining the enhanced features, we introduce the multi linear heads, which utilizes multiple decoder heads for different attributes in the Gaussian. Since the coordinates of the point cloud and the Gaussian are not exactly the same in space, we take inspiration from [63] and learn the positional offset of the Gaussians concerning the point cloud, instead of the centers themselves, to simplify the learning process. Details of the Point-to-Gaussian Decoder are provided in the supplementary materials (Tab. 1).

3.3 Cross Modality Enhancement

In this section, we present the core component of our Point to Gaussian generator, which integrate the 3D representations obtained from the Attention mechanism, Projection mechanism, and Point feature extractor, termed as APP, for cross modality enhancement, as shown in Fig. 3. The point feature extractor we employ is based on PVCNN [23], which extracts the geometry and texture feature from the colored point cloud. Despite employing a multi-scale feature extraction module to provide a larger receptive field, the features extracted from point cloud input remain carry insufficient appearance features and inaccurate geometry structural information to provide informative prior for precise Gaussian generation. To further integrate the rich texture from the image modality into the point cloud tokens, we designed projection and attention modules which will be discussed in the following subsections.

3.3.1 Projection. Numerous studies have been conducted in multi-modal fusion, where an efficient and intuitive approach is projection. Inspired by this, we fuse multi-scale point cloud tokens with image tokens using projection, complementing each point cloud with a feature from the image modality based on its position in space and the view of the input image. Specifically, we use the method mentioned in [31] for the projection process which considers that the point cloud is volumetric and non-transparent in space and employs a fast rasterization technique to map the pixel-wise image features to the visible points.

However, considering that the point cloud is assumed to be volumetric and non-transparent during the rasterization process, it is inevitable that points opposing the current camera viewpoint will be invisible during this process. As illustrated in Fig. 4, in the two provided viewpoints on the left side, we can only observe one side of the character, implying that the occluded point cloud on the other side will not participate in the projection process.

3.3.2 Attention. To further compensate for the point clouds that are against the current projection view, we propose using the attention mechanism to enhance the point cloud features further. Specifically, the point cloud features and image features interact via cross-attention, which further fuses the features of both modalities. It is worth noting that we do not explicitly define the mapping between the point cloud and the image but encourage the network itself to model the positional relationship between them. This approach differs from the projection process, where we align the point cloud and image based on the camera parameters and then explicitly fuse them.

This implicit fusion enables all points in the space to be augmented with image features obtained from DINOv2 [35]. Assuming the point cloud tokens are T_p , which are treated as the query, and the image tokens are T_i , which as key and value. The point cloud features interact with all the image tokens globally to obtain the output, which can be expressed as:

$$T_{att} = \text{CrossAtt}(T_p, T_i, T_i) \quad (6)$$

3.3.3 Aggregation. To enhance the features of the point cloud, we introduce projection and attention mechanisms for cross modality enhancement, respectively. Finally, we aggregate the enhanced

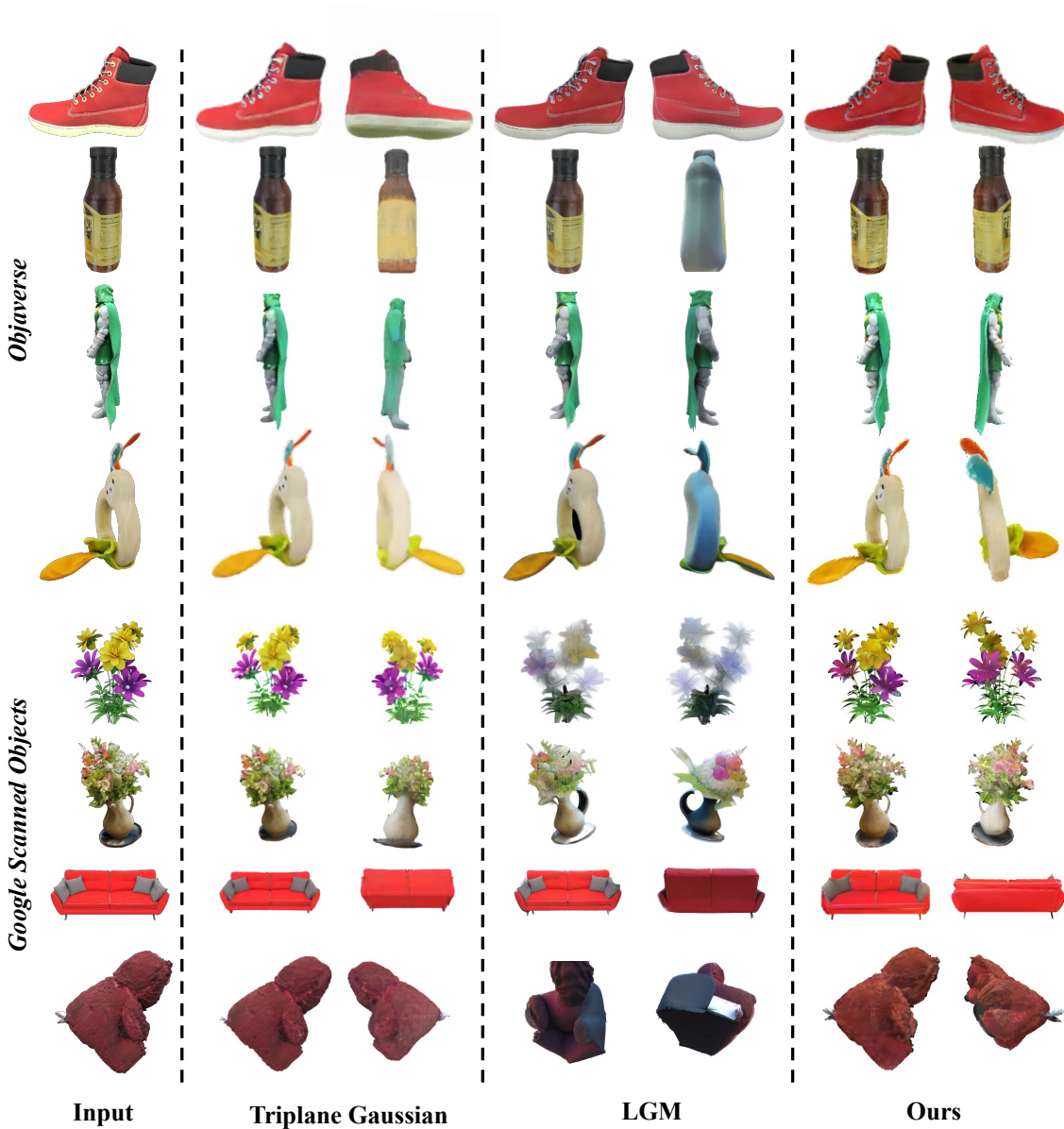


Figure 5: Qualitative results among baselines of single view image-to-3D reconstruction on Objaverse [9] and Google Scanned Objects [10] dataset. Our method outperforms previous Gaussian based baselines in both geometry and texture, and in particular our method generates more consistent multi-view renderings, thanks to the geometry prior of the point cloud input.

features using average aggregation:

$$T_{out} = Avg(T_p, T_{pro}, T_{att}) \quad (7)$$

3.4 Optimization

3.4.1 Training Loss. The Gaussian generator is trained using rendering loss. In each iteration, we randomly select M views, with one serving as the conditional input, while the remaining $M - 1$ views are employed for supervision. Following the methodology of prior research [44], we compute the photometric loss and alpha

loss between the rendered image and the ground truth image. Our objective is to minimize the following objective function.

$$L = L_{pixel} + \lambda_{pc} L_{pc} \quad (8)$$

$$L_{pc} = L_{cd} + L_{emd} \quad (9)$$

$$L_{pixel} = L_{MSE}^{rgb} + \lambda_{LPIPS} L_{LPIPS}^{rgb} + \lambda_{\alpha} L_{MSE}^{\alpha} \quad (10)$$

where λ_{LPIPS} and λ_{α} are corresponding weight coefficient, and L_{LPIPS} are perceptual image patch similarity [60].

Table 1: Qualitative rendering results on single-view image-to-3D. We compare the reconstruction quality for 32 novel views with 100 random objects selected from GSO [10]. Our method outperformed relevant feed-forward based generation baselines with comparable inference speed. The best results are bolded.

	PSNR \uparrow	SSIM \uparrow	LPIPS \downarrow	Time \downarrow
One-2-3-45 [20]	17.54	0.80	0.21	~ 50s
Point-E [34]	15.50	0.69	0.37	~ 7s
LRM [12]	16.09	0.79	0.28	~ 6s
TriplaneGaussian [63]	16.15	0.82	0.27	~ 1s
LGM [44]	17.13	0.81	0.25	~ 6s
Ours	17.92	0.81	0.21	~ 7s

3.4.2 Data Augmentation. During training, we use point cloud data from ground truth (GT), but when inference, the model inputs are generated from the 3D diffusion model. To mitigate the gap in data distributions, we perturb the point cloud data when training the model using data augmentation. Specifically, we jitter the coordinates and RGB values of the input point cloud by adding noise to them, thereby enhancing the robustness of the model to the input.

4 Experiments

In this section, we initially delve into the specifics of the experiments, followed by a discussion on the dataset employed in our training and testing. Then we present our experimental results, offering both qualitative and quantitative analyses between ours and other methods. We conduct an ablation study to validate the effectiveness of our proposed modules lastly.

4.1 Implementation Details

The 3D diffusion model we deployed is Point-E [34], which presents commendable performance. Alternative methods for obtaining point clouds, such as DUST3R [50], sparse reconstruction [25], or even 3D scanners, can also be utilized. The implementation of point cloud upsampler is based on the SPD module proposed in SnowflakeNet [52], which takes a 4K input and generates a 16K point cloud output. The image encoder utilized is the pretrained DINOv2 [35], and the architecture of our Point to Gaussian generator is based on the [23], with both the encoder and decoder consisting of four layers. Besides, to conserve computational resources, we incorporate the APP module solely into the encoder during the training process. The loss weights for mask and LPIPS losses are both set to 1. Meanwhile, the loss weights for point clouds are gradually attenuated from 1 to 0.05 using cosine annealing. During the training process, the number of views per iteration was set to 4 (i.e., $M = 4$). The experiment was conducted with 16 NVIDIA Tesla A100 GPUs for training, spanning approximately 3 days. The resolution of novel view rendering was 256, with a batch size of 128 (batch size 8 for each GPU).

4.2 Dataset

The model is trained on the Objaverse-LVIS [9] dataset. We render RGB images from 32 perspectives by rotating around the object’s

Table 2: Ablation study on our proposed APP block. The best results are bolded.

Point Feature Extractor	Attention	Projection	PSNR \uparrow	SSIM \uparrow	LPIPS \downarrow
✓			15.84	0.72	0.31
✓		✓	17.17	0.78	0.22
✓	✓		17.25	0.80	0.25
✓	✓	✓	17.92	0.81	0.21

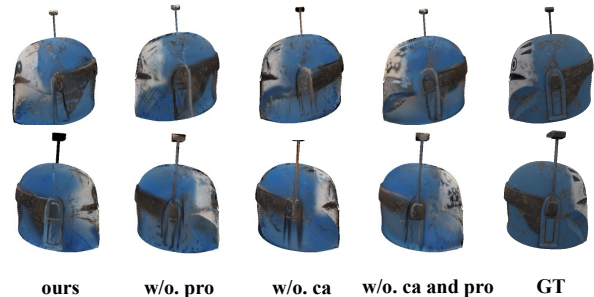


Figure 6: Visualization of effects inside the proposed APP block. w/o. pro represents removing projection mechanism, and w/o. ca represents removing cross-attention mechanism. The w/o. ca and pro represents that the APP block contains only point feature extractor.

surface, which is similar to [42]. Regarding the point cloud, we utilized the point cloud data provided by [26]. Through farthest point sampling, we obtained a 4k point cloud as the input. We evaluate our methods on the Objaverse and Google Scanned Objects [10] and randomly selected 100 test samples from each of the two datasets, respectively. Specifically, we input one view and evaluate it on 32 rendering views.

4.3 Results

4.3.1 Qualitative Comparison. We predominantly compare our approach with recent Gaussian-based 3D generation methods on the Objaverse [9] and Google Scanned Objects [10]. The qualitative comparison of the results is depicted in Fig. 5. As observed, our method demonstrates richer high-frequency details compared to other models for both datasets. More qualitative comparison results could be found in supplementary materials.

Reconstructing the backside view is a formidable challenge, as demonstrated by the results of LGM in the **Second** line. The results for the backside of the bottle appear inconsistent with the input view. However, our results exhibit remarkable consistency, and our results more accurately recover the content from the input view, yielding more coherent and reasonable geometry and texture details. This improvement can be ascribed to the cross modality enhancement, which fuses image tokens in multiple scales.

4.3.2 Quantitative Comparison. We also carried out a quantitative comparison with other methodologies and calculate Peak Signal-to-Noise Ratio (PSNR), Structural Similarity Index (SSIM), and Learned Perceptual Image Patch Similarity (LPIPS) [60] metrics to assess the quality of images. The quantitative results are presented in Table 1.

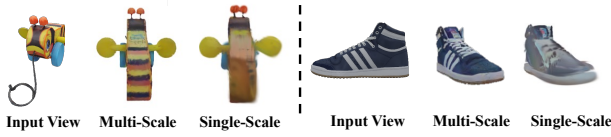


Figure 7: Cross Modality Enhancement with single-scale and multi-scale fusion.

As evident from the table, our method surpasses other feed-forward methods in terms of generation quality across all metrics, while maintaining a comparable inference speed. The time intensity of our process is primarily attributed to the initial stage of point cloud acquisition, as can be deduced by comparing our time usage with that of Point-E. However, in the second stage, the Point-to-Gaussian Generator can be inferred in real-time due to fast rendering speed.

4.4 Ablation Study

4.4.1 APP Block. We first trained a baseline model using the point feature extractor only. Based on it, we added projection and attention respectively. The quantitative experimental results are presented in Table 2, which indicates the projection and attention we designed can significantly facilitate the learning of Gaussian attributes. Moreover, when both mechanism are employed, which further enhances the performance. A qualitative comparison of the results, is shown in Fig. 6, which also demonstrates that the quality of the reconstructed images is significantly improved.

4.4.2 Multi-Scale Enhancement. We implemented an ablation study to evaluate the effectiveness of the multi-scale fusion strategy in our proposed Cross Modality Enhancement. Specifically, we trained a baseline model without multi-scale fusing by removing the FPS operation. The results of this study are presented in Fig. 7, which clearly demonstrate that the proposed multi-scale fusion strategy significantly improves the coherence of texture details in the novel views.

Our proposed APP block fuses image features and point cloud features at multi-scale. This is different from previous works that attend the image feature to triplane in single-scale, such as LRM [12], Triplane Gaussian [63]. Our architecture builds a hierarchical grouping of points and progressively abstracts larger local regions, which summarizes the context between frontside and backside points. Therefore, the backside point tokens gain more contextual information from 2D features than the single-scale fusing method.

4.4.3 Number of Views. With the assistance of existing multi-view diffusion model ImageDream [48], our method also supports multi-image input. Specifically, we first convert the single image into four consistent images, and then feed them into the Gaussian generator. Table 3 indicates that more image inputs further improve the reconstruction quality. The qualitative results in Fig. 8 also support this conclusion, as the reconstructed image with multi-image input exhibits better clarity and geometric consistency.

4.4.4 Learning Offsets for Gaussian Centers. We ablate on the strategy of learning offsets for Gaussian center and visualize the rendered images and 3D Gaussians at different iterations, as displayed in Fig. 9. The top row presents the outcome of direct Gaussian

Table 3: Ablation study on the number of input views.

	Single View	Multi View
PSNR \uparrow	17.92	18.09
SSIM \uparrow	0.81	0.82
LPIPS \downarrow	0.21	0.19



Figure 8: Visualization of rendered images and 3D Gaussians. We present the effect of different numbers of input views.

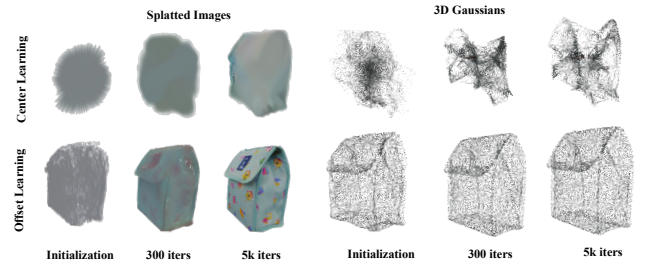


Figure 9: Visualization of the training process. The first row represents that Gaussian centers are directly regressed while the second row is the learning of Gaussian centers' offsets.

centers learning. At the beginning of training, the 3D Gaussians are predominantly characterized by noise, and the model requires approximately 5k iterations before revealing the basic shape of the bag. In contrast, with offset learning, as depicted in the bottom row, the 3D Gaussians exhibit good geometry during the initial training and demonstrate faster convergence speed. After just 300 iterations, the model can reconstruct the basic geometry of the input object. With offset learning, the Gaussians can be initialized to a suitable position by the point cloud at the beginning of training.

5 Conclusion

In this paper, we present a large point-to-Gaussian model for image-to-3D generation. Point-to-Gaussian model inputs point cloud to generate Gaussian parameters, in which the input point cloud is generated from a large 3D diffusion model (e.g. Point-E) from the 2D image. With the geometry prior from point cloud, Point-to-Gaussian model is able to significantly improve image-to-3D generation. In addition, based on a multi-scale network, we further devise a APP block, which fuse the image features into point cloud representations with an attention mechanism and pose-aware projection mechanism. Extensive experiments demonstrate the effectiveness of the proposed approach on GSO and Objaverse datasets, and the proposed method achieves state-of-the-art performance.

Acknowledgments

This work is supported in part by the National Natural Science Foundation of China, under Grant (62302309,62171248), Shenzhen Science and Technology Program (JCYJ20220818101014030, JCYJ20220818101012025), and the PCNL KEY project (PCL2023AS6-1).

References

- [1] David Charatan, Sizhe Li, Andrea Tagliasacchi, and Vincent Sitzmann. 2023. pixelsplat: 3d gaussian splats from image pairs for scalable generalizable 3d reconstruction. *arXiv preprint arXiv:2312.12337* (2023).
- [2] Hansheng Chen, Jiatao Gu, Anpei Chen, Wei Tian, Zhuowen Tu, Lingjie Liu, and Hao Su. 2023. Single-stage diffusion nerf: A unified approach to 3d generation and reconstruction. In *Proceedings of the IEEE/CVF International Conference on Computer Vision*. 2416–2425.
- [3] Rui Chen, Yongwei Chen, Ningxin Jiao, and Kui Jia. 2023. Fantasia3d: Disentangling geometry and appearance for high-quality text-to-3d content creation. In *Proceedings of the IEEE/CVF International Conference on Computer Vision*. 22246–22256.
- [4] Yuedong Chen, Haofei Xu, Chuanxia Zheng, Bohan Zhuang, Marc Pollefeys, Andreas Geiger, Tat-Jen Cham, and Jianfei Cai. 2024. MVSplat: Efficient 3D Gaussian Splatting from Sparse Multi-View Images. *arXiv preprint arXiv:2403.14627* (2024).
- [5] Zilong Chen, Feng Wang, and Huaping Liu. 2023. Text-to-3d using gaussian splatting. *arXiv preprint arXiv:2309.16585* (2023).
- [6] Zilong Chen, Feng Wang, and Huaping Liu. 2023. Text-to-3d using gaussian splatting. *arXiv preprint arXiv:2309.16585* (2023).
- [7] Zilong Chen, Yikai Wang, Feng Wang, Zhengyi Wang, and Huaping Liu. 2024. V3D: Video Diffusion Models are Effective 3D Generators. *arXiv preprint arXiv:2403.06738* (2024).
- [8] Matt Deitke, Ruoshi Liu, Matthew Wallingford, Huong Ngo, Oscar Michel, Aditya Kusupati, Alan Fan, Christian Laforte, Vikram Voleti, Samir Yitzhak Gadre, et al. 2024. Objaverse-xl: A universe of 10m+ 3d objects. *Advances in Neural Information Processing Systems* 36 (2024).
- [9] Matt Deitke, Dustin Schwenk, Jordi Salvador, Luca Weihs, Oscar Michel, Eli VanderBilt, Ludwig Schmidt, Kiana Ehsani, Aniruddha Kembhavi, and Ali Farhadi. 2023. Objaverse: A universe of annotated 3d objects. In *Proceedings of the IEEE/CVF Conference on Computer Vision and Pattern Recognition*. 13142–13153.
- [10] Laura Downs, Anthony Francis, Nate Koenig, Brandon Kinman, Ryan Hickman, Krista Reymann, ThomasB. McHugh, and Vincent Vanhoucke. 2022. Google Scanned Objects: A High-Quality Dataset of 3D Scanned Household Items. (Apr 2022).
- [11] Huachen Gao, Shihe Shen, Zhe Zhang, Kaiqiang Xiong, Rui Peng, Zhirui Gao, Qi Wang, Yugui Xie, and Ronggang Wang. 2024. FDC-NeRF: Learning Pose-Free Neural Radiance Fields with Flow-Depth Consistency. In *ICASSP 2024 - 2024 IEEE International Conference on Acoustics, Speech and Signal Processing (ICASSP)*. 3615–3619.
- [12] Yicong Hong, Kai Zhang, Jiuxiang Gu, Sai Bi, Yang Zhou, Difan Liu, Feng Liu, Kalyan Sunkavalli, Trung Bui, and Hao Tan. 2023. Lrm: Large reconstruction model for single image to 3d. *arXiv preprint arXiv:2311.04400* (2023).
- [13] Heewoo Jun and Alex Nichol. 2023. Shap-e: Generating conditional 3d implicit functions. *arXiv preprint arXiv:2305.02463* (2023).
- [14] Bernhard Kerbl, Georgios Kopanas, Thomas Leimkuehler, and George Drettakis. 2023. 3D Gaussian Splatting for Real-Time Radiance Field Rendering. *ACM Transactions on Graphics (TOG)* 42, 4 (2023), 1–14.
- [15] Jiahao Li, Hao Tan, Kai Zhang, Zexiang Xu, Fujun Luan, Yinghao Xu, Yicong Hong, Kalyan Sunkavalli, Greg Shakhnarovich, and Sai Bi. 2023. Instant3d: Fast text-to-3d with sparse-view generation and large reconstruction model. *arXiv preprint arXiv:2311.06214* (2023).
- [16] Weiyu Li, Rui Chen, Xuelin Chen, and Ping Tan. 2023. Sweetdreamer: Aligning geometric priors in 2d diffusion for consistent text-to-3d. *arXiv preprint arXiv:2310.02596* (2023).
- [17] Chen-Hsuan Lin, Jun Gao, Luming Tang, Towaki Takikawa, Xiaohei Zeng, Xun Huang, Karsten Kreis, Sanja Fidler, Ming-Yu Liu, and Tsung-Yi Lin. 2023. Magic3d: High-resolution text-to-3d content creation. In *Proceedings of the IEEE/CVF Conference on Computer Vision and Pattern Recognition*. 300–309.
- [18] Huan Ling, Seung Wook Kim, Antonio Torralba, Sanja Fidler, and Karsten Kreis. 2023. Align your gaussians: Text-to-4d with dynamic 3d gaussians and composed diffusion models. *arXiv preprint arXiv:2312.13763* (2023).
- [19] Minghua Liu, Ruoxi Shi, Linghao Chen, Zhuoyang Zhang, Chao Xu, Xinyue Wei, Hansheng Chen, Chong Zeng, Jiayuan Gu, and Hao Su. 2023. One-2-3-45++: Fast single image to 3d objects with consistent multi-view generation and 3d diffusion. *arXiv preprint arXiv:2311.07885* (2023).
- [20] Minghua Liu, Chao Xu, Haiyan Jin, Linghao Chen, Mukund Varma T, Zexiang Xu, and Hao Su. 2024. One-2-3-45: Any single image to 3d mesh in 45 seconds without per-shape optimization. *Advances in Neural Information Processing Systems* 36 (2024).
- [21] Ruoshi Liu, Rundi Wu, Basile Van Hoorick, Pavel Tokmakov, Sergey Zakharov, and Carl Vondrick. 2023. Zero-1-to-3: Zero-shot one image to 3d object. In *Proceedings of the IEEE/CVF International Conference on Computer Vision*. 9298–9309.
- [22] Zexiang Liu, Yangguang Li, Youtian Lin, Xin Yu, Sida Peng, Yan-Pei Cao, Xiaojuan Qi, Xiaoshui Huang, Ding Liang, and Wanli Ouyang. 2023. UniDream: Unifying Diffusion Priors for Relightable Text-to-3D Generation. *arXiv preprint arXiv:2312.08754* (2023).
- [23] Zhijian Liu, Haotian Tang, Yujun Lin, and Song Han. 2019. Point-voxel cnn for efficient 3d deep learning. *Advances in neural information processing systems* 32 (2019).
- [24] Xiaoxiao Long, Yuan-Chen Guo, Cheng Lin, Yuan Liu, Zhiyang Dou, Lingjie Liu, Yuxin Ma, Song-Hai Zhang, Marc Habermann, Christian Theobalt, et al. 2023. Wonder3d: Single image to 3d using cross-domain diffusion. *arXiv preprint arXiv:2310.15008* (2023).
- [25] Xiaoxiao Long, Cheng Lin, Peng Wang, Taku Komura, and Wenping Wang. 2022. Sparseneus: Fast generalizable neural surface reconstruction from sparse views. In *European Conference on Computer Vision*. Springer, 210–227.
- [26] Tiange Luo, Chris Rockwell, Honglak Lee, and Justin Johnson. 2024. Scalable 3d captioning with pretrained models. *Advances in Neural Information Processing Systems* 36 (2024).
- [27] Baorui Ma, Haoge Deng, Junsheng Zhou, Yu-Shen Liu, Tiejun Huang, and Xinlong Wang. 2023. Geodream: Disentangling 2d and geometric priors for high-fidelity and consistent 3d generation. *arXiv preprint arXiv:2311.17971* (2023).
- [28] Baorui Ma, Zhizhong Han, Yu-Shen Liu, and Matthias Zwicker. 2021. Neural-Pull: Learning Signed Distance Function from Point clouds by Learning to Pull Space onto Surface. In *International Conference on Machine Learning*. PMLR, 7246–7257.
- [29] Baorui Ma, Yu-Shen Liu, and Zhizhong Han. 2022. Reconstructing Surfaces for Sparse Point Clouds with On-Surface Priors. In *Proceedings of the IEEE/CVF Conference on Computer Vision and Pattern Recognition*.
- [30] Baorui Ma, Yu-Shen Liu, Matthias Zwicker, and Zhizhong Han. 2022. Surface Reconstruction from Point Clouds by Learning Predictive Context Priors. In *Proceedings of the IEEE/CVF Conference on Computer Vision and Pattern Recognition*.
- [31] Luke Melas-Kyriazi, Christian Rupprecht, and Andrea Vedaldi. 2023. Pc2: Projection-conditioned point cloud diffusion for single-image 3d reconstruction. In *Proceedings of the IEEE/CVF Conference on Computer Vision and Pattern Recognition*. 12923–12932.
- [32] Gal Metzger, Elad Richardson, Or Patashnik, Raja Giryes, and Daniel Cohen-Or. 2023. Latent-nerf for shape-guided generation of 3d shapes and textures. In *Proceedings of the IEEE/CVF Conference on Computer Vision and Pattern Recognition*. 12663–12673.
- [33] Ben Mildenhall, Pratul P Srinivasan, Matthew Tancik, Jonathan T Barron, Ravi Ramamoorthi, and Ren Ng. 2020. NeRF: Representing Scenes as Neural Radiance Fields for View Synthesis. In *European Conference on Computer Vision*. Springer, 405–421.
- [34] Alex Nichol, Heewoo Jun, Prafulla Dhariwal, Pamela Mishkin, and Mark Chen. 2022. Point-e: A system for generating 3d point clouds from complex prompts. *arXiv preprint arXiv:2212.08751* (2022).
- [35] Maxime Oquab, Timothée Darcet, Théo Moutakanni, Huy Vo, Marc Szafraniec, Vasil Khalidov, Pierre Fernandez, Daniel Haziza, Francisco Massa, Alaaeldin El-Nouby, et al. 2023. Dinov2: Learning robust visual features without supervision. *arXiv preprint arXiv:2304.07193* (2023).
- [36] Rui Peng, Xiaodong Gu, Luyang Tang, Shihe Shen, Fanqi Yu, and Ronggang Wang. 2023. Gens: Generalizable neural surface reconstruction from multi-view images. *Advances in Neural Information Processing Systems* 36 (2023), 56932–56945.
- [37] Rui Peng, Rongjie Wang, Zhenyu Wang, Yawen Lai, and Ronggang Wang. 2022. Rethinking depth estimation for multi-view stereo: A unified representation. In *Proceedings of the IEEE/CVF conference on computer vision and pattern recognition*. 8645–8654.
- [38] Ben Poole, Ajay Jain, Jonathan T Barron, and Ben Mildenhall. 2022. Dreamfusion: Text-to-3d using 2d diffusion. *arXiv preprint arXiv:2209.14988* (2022).
- [39] Robin Rombach, Andreas Blattmann, Dominik Lorenz, Patrick Esser, and Björn Ommer. 2022. High-resolution image synthesis with latent diffusion models. In *Proceedings of the IEEE/CVF conference on computer vision and pattern recognition*. 10684–10695.
- [40] Junyoung Seo, Wooseok Jang, Min-Seop Kwak, Hyeonsu Kim, Jaehoon Ko, Junho Kim, Jin-Hwa Kim, Jiyoung Lee, and Seungryong Kim. 2023. Let 2d diffusion model know 3d-consistency for robust text-to-3d generation. *arXiv preprint arXiv:2303.07937* (2023).
- [41] Ruoxi Shi, Hansheng Chen, Zhuoyang Zhang, Minghua Liu, Chao Xu, Xinyue Wei, Linghao Chen, Chong Zeng, and Hao Su. 2023. Zero123++: a single image to consistent multi-view diffusion base model. *arXiv preprint arXiv:2310.15110* (2023).

- [42] Yichun Shi, Peng Wang, Jianglong Ye, Mai Long, Kejie Li, and Xiao Yang. 2023. Mv-dream: Multi-view diffusion for 3d generation. [arXiv preprint arXiv:2308.16512](#) (2023).
- [43] Stanisław Szymanowicz, Christian Rupprecht, and Andrea Vedaldi. 2023. Splatter image: Ultra-fast single-view 3d reconstruction. [arXiv preprint arXiv:2312.13150](#) (2023).
- [44] Jiaxiang Tang, Zhaoxi Chen, Xiaokang Chen, Tengfei Wang, Gang Zeng, and Ziwei Liu. 2024. LGM: Large Multi-View Gaussian Model for High-Resolution 3D Content Creation. [arXiv preprint arXiv:2402.05054](#) (2024).
- [45] Jiaxiang Tang, Jiawei Ren, Hang Zhou, Ziwei Liu, and Gang Zeng. 2023. Dream-gaussian: Generative gaussian splatting for efficient 3d content creation. [arXiv preprint arXiv:2309.16653](#) (2023).
- [46] Vikram Voleti, Chun-Han Yao, Mark Boss, Adam Letts, David Pankratz, Dmitry Tochilkin, Christian Laforte, Robin Rombach, and Varun Jampani. 2024. Sv3d: Novel multi-view synthesis and 3d generation from a single image using latent video diffusion. [arXiv preprint arXiv:2403.12008](#) (2024).
- [47] Haochen Wang, Xiaodan Du, Jiahao Li, Raymond A Yeh, and Greg Shakhnarovich. 2023. Score jacobian chaining: Lifting pretrained 2d diffusion models for 3d generation. In *Proceedings of the IEEE/CVF Conference on Computer Vision and Pattern Recognition*. 12619–12629.
- [48] Peng Wang and Yichun Shi. 2023. Imagedream: Image-prompt multi-view diffusion for 3d generation. [arXiv preprint arXiv:2312.02201](#) (2023).
- [49] Peng Wang, Hao Tan, Sai Bi, Yinghao Xu, Fujun Luan, Kalyan Sunkavalli, Wenping Wang, Zexiang Xu, and Kai Zhang. 2023. Pf-lrm: Pose-free large reconstruction model for joint pose and shape prediction. [arXiv preprint arXiv:2311.12024](#) (2023).
- [50] Shuzhe Wang, Vincent Leroy, Yohann Cabon, Boris Chidlovskii, and Jerome Revaud. 2023. DUST3R: Geometric 3D Vision Made Easy. [arXiv preprint arXiv:2312.14132](#) (2023).
- [51] Zhengyi Wang, Cheng Lu, Yikai Wang, Fan Bao, Chongxuan Li, Hang Su, and Jun Zhu. 2024. Prolificdreamer: High-fidelity and diverse text-to-3d generation with variational score distillation. *Advances in Neural Information Processing Systems* 36 (2024).
- [52] Peng Xiang, Xin Wen, Yu-Shen Liu, Yan-Pei Cao, Pengfei Wan, Wen Zheng, and Zhizhong Han. 2021. Snowflakenet: Point cloud completion by snowflake point deconvolution with skip-transformer. In *Proceedings of the IEEE/CVF international conference on computer vision*. 5499–5509.
- [53] DeJia Xu, Ye Yuan, Morteza Mardani, Sifei Liu, Jiaming Song, Zhangyang Wang, and Arash Vahdat. 2024. Agg: Amortized generative 3d gaussians for single image to 3d. [arXiv preprint arXiv:2401.04099](#) (2024).
- [54] Jiale Xu, Xintao Wang, Weihao Cheng, Yan-Pei Cao, Ying Shan, Xiaohu Qie, and Shenghua Gao. 2023. Dream3d: Zero-shot text-to-3d synthesis using 3d shape prior and text-to-image diffusion models. In *Proceedings of the IEEE/CVF Conference on Computer Vision and Pattern Recognition*. 20908–20918.
- [55] Yinghao Xu, Hao Tan, Fujun Luan, Sai Bi, Peng Wang, Jiahao Li, Zifan Shi, Kalyan Sunkavalli, Gordon Wetzstein, Zexiang Xu, et al. 2023. Dmv3d: Denoising multi-view diffusion using 3d large reconstruction model. [arXiv preprint arXiv:2311.09217](#) (2023).
- [56] Taoran Yi, Jiemin Fang, Guanjun Wu, Lingxi Xie, Xiaopeng Zhang, Wenyu Liu, Qi Tian, and Xinggang Wang. 2023. Gaussiandreamer: Fast generation from text to 3d gaussian splatting with point cloud priors. [arXiv preprint arXiv:2310.08529](#) (2023).
- [57] Yaohua Zha, Huizhen Ji, Jinmin Li, Rongsheng Li, Tao Dai, Bin Chen, Zhi Wang, and Shu-Tao Xia. 2024. Towards compact 3d representations via point feature enhancement masked autoencoders. In *Proceedings of the AAAI Conference on Artificial Intelligence*, Vol. 38. 6962–6970.
- [58] Yaohua Zha, Naiqi Li, Yanzi Wang, Tao Dai, Hang Guo, Bin Chen, Zhi Wang, Zhihao Ouyang, and Shu-Tao Xia. 2024. LCM: Locally Constrained Compact Point Cloud Model for Masked Point Modeling. [arXiv preprint arXiv:2405.17149](#) (2024).
- [59] Yaohua Zha, Jinpeng Wang, Tao Dai, Bin Chen, Zhi Wang, and Shu-Tao Xia. 2023. Instance-aware dynamic prompt tuning for pre-trained point cloud models. In *Proceedings of the IEEE/CVF International Conference on Computer Vision*. 14161–14170.
- [60] Richard Zhang, Phillip Isola, Alexei A Efros, Eli Shechtman, and Oliver Wang. 2018. The unreasonable effectiveness of deep features as a perceptual metric. In *Proceedings of the IEEE conference on computer vision and pattern recognition*. 586–595.
- [61] Shunyuhan Zheng, Boyao Zhou, Ruizhi Shao, Boning Liu, Shengping Zhang, Liqiang Nie, and Yebin Liu. 2023. Gps-gaussian: Generalizable pixel-wise 3d gaussian splatting for real-time human novel view synthesis. [arXiv preprint arXiv:2312.02155](#) (2023).
- [62] Junsheng Zhou, Jinsheng Wang, Baorui Ma, Yu-Shen Liu, Tiejun Huang, and Xinlong Wang. 2024. Uni3D: Exploring Unified 3D Representation at Scale. *International Conference on Learning Representations* (2024).
- [63] Zi-Xin Zou, Zhipeng Yu, Yuan-Chen Guo, Yangguang Li, Ding Liang, Yan-Pei Cao, and Song-Hai Zhang. 2023. Triplane meets gaussian splatting: Fast and generalizable single-view 3d reconstruction with transformers. [arXiv preprint arXiv:2312.09147](#) (2023).